Original papers
Nanostructured, nanoscale materials and nanodevices

УДК 53.043, 532.6 DOI: 10.17277/jamt.2022.01.pp.058-067

The control of ITO conductive coating relief via laser-oriented deposited carbon nanotubes

Andrei S. Toikka[a,b,c]✉, Natalia V. Kamanina[a,b,c]

[a] *Vavilov State Optical Institute, 5/2, Kadetskaya St., St. Petersburg 199053, Russian Federation,*
[b] *Saint Petersburg Electrotechnical University,*
5, Professora Popova St., St. Petersburg 197376, Russian Federation,
[c] *Petersburg Nuclear Physics Institute named by B.P. Konstantinov of National Research Centre "Kurchatov Institute",*
1, Orlova roscha St., Gatchina 188300, Russian Federation

✉ atoikka@obraz.pro

Abstract: The paper presents the analysis of the surface relief of ITO conductive layers structured with single-walled carbon nanotubes. The deposition of ITO films and carbon nanotubes was carried out by laser-oriented method using a CO_2 laser. The optical scheme was matched to the control electric grid; the strength of the electric field was varied in the range of 100–600 V·cm^{-1}. To analyze the surface, atomic force microscopy in the contact mode and measurement of the wetting angle by sessile drop method was used. Roughness of pure ITO was about 1.8 nm, while in laser-vacuum deposition of carbon nanotubes, roughness varied from 6.4 nm to 22.1 nm with an increase in the electric field during deposition. The relationship between roughness and surface area of coatings and the wetting angle was considered. An increase in the wetting angle from 101.8 degrees, in the case of pure ITO, to 115.0-128.6 degrees, with the deposition of carbon nanotubes, was shown. The results obtained indicate an improvement in the resistance of ITO coatings to moisture during the deposition of carbon nanotubes, which makes it possible to expand their operating conditions and scope in optical electronics, laser and display technology.

Keywords: laser-oriented deposition technique; indium and tin oxides; surface structurization; wetting angle; sessile drop method.

For citation: Toikka AS, Kamanina NV. The control of ITO conductive coating relief via laser-oriented deposited carbon nanotubes. *Journal of Advanced Materials and Technologies*. 2022;7(1):58-67. DOI: 10.17277/jamt.2022.01.pp.058-067

Управление рельефом проводящих ITO-покрытий при помощи лазерно-ориентированного осаждения углеродных нанотрубок

А. С. Тойкка[a,b,c]✉, Н. В. Каманина[a,b,c]

[a] *Государственный оптический институт им. С. И. Вавилова,*
Кадетская линия, 5/2, Санкт-Петербург 199053, Российская Федерация,
[b] *Санкт-Петербургский государственный электротехнический университет «ЛЭТИ» им. В. И. Ульянова (Ленина),*
ул. Профессора Попова, 5, Санкт-Петербург 197376, Российская Федерация,
[c] *Петербургский институт ядерной физики им. Б. П. Константинова Национального исследовательского центра «Курчатовский институт», Орлова Роща, 1, Гатчина 188300, Российская Федерация*

✉ atoikka@obraz.pro

Аннотация: Представлен анализ рельефа поверхности проводящих контактов на основе ITO, структурированных одностенными углеродными нанотрубками. Осаждение пленок ITO и углеродных нанотрубок проводилось лазерно-ориентированным методом с использованием CO_2-лазера. Оптическая схема была согласована с управляющей электрической сеткой, напряженность поля варьировалась в диапазоне 100…600 В/см. Для диагностики поверхности последовательно использовались атомно-силовая микроскопия в контактном режиме и измерение краевого угла смачивания методом висячей капли. Шероховатость чистого ITO составила порядка 1,8 нм, в то время как при лазерно-вакуумном осаждении углеродных нанотрубок шероховатость

варьировалась от 6,4 до 22,1 нм с ростом электрического поля в процессе напыления. Рассматривалась связь шероховатости и площади поверхности покрытий с краевым углом смачивания. Показан рост угла смачивания от 101,8° в случае чистого ITO до 115,0…128,6° при осаждении углеродных нанотрубок. Полученные результаты свидетельствуют об улучшении стойкости ITO-покрытий к влаге при осаждении углеродных нанотрубок, что позволяет расширить их условия эксплуатации и область применения в оптической электронике, лазерной и дисплейной технике.

Ключевые слова: метод лазерно-ориентированного осаждения; оксиды индия и олова; структурирование поверхности; краевой угол смачивания; метод висячей капли.

Для цитирования: Toikka AS, Kamanina NV. The control of ITO conductive coating relief via laser-oriented deposited carbon nanotubes. *Journal of Advanced Materials and Technologies*. 2022;7(1):58-67. DOI: 10.17277/jamt.2022.01.pp.058-067

1. Introduction

Along with functional photosensitive and modulating layers of optoelectronic devices, indium and tin oxides (ITO) are one of the key semiconductor materials in electronics, which, depending on the field of application of the developed system, can function both as transparent conductive contacts, antireflection coatings and buffer coatings [1–5]. ITO coatings are transparent in the visible and near infrared spectrum regions, flexible, non-toxic, and have a relatively high conductivity, which allows them to be used in photovoltaics [6–9], flexible electronics [10–13], and display technologies [14–17].

It should be noted that the content of indium in the Earth's crust is limited, and its cost is slowly but gradually increasing, therefore, in electronics, ITO is currently partially replaced by tin oxides with fluorine (FTO) [18–19], zinc oxides (ZnO), and zinc oxides with aluminum (AZO) [20–22], as well as using other materials [23–27]. Despite this, ITO is still in demand due to the possibility of optical refractive index matching with silicon, liquid crystals, and glass [28–33]. In photovoltaics, the ITO layer should reduce reflection losses and also accumulate charge carriers. In liquid-crystal technologies, contacts are made on the basis of this material at the interface: solid-liquid crystal. The ITO-glass tandem is used to protect against freezing, for example, car windshields.

Obtaining and controlled switching of the desired properties of ITO coatings often depends on the deposition method. In vacuum methods, for example, in magnetron sputtering and thermoresistive deposition, it is done by varying the power and oxygen concentration [34–38]. In chemical methods, for example, in sol-gel centrifugation, the rotation frequency and solvent composition are changed to control the ITO properties [39]. It is worth noting that thermal annealing is widely used in most methods [40–41].

In our study, we continue to improve the method of laser deposition of carbon nanotubes on the surface of various materials, including ITO [42–44]. Thus, in this work, the method of laser-oriented deposition of single-walled carbon nanotubes (CNTs) [45] is used to change the ITO parameters. The refractive index of CNTs (at the level of 1.05–1.10) is lower than that of ITO, which makes it possible to reduce reflection losses. CNTs with metallic chirality significantly reduce the electrical resistance of ITO [46]. Since they have a high Young's modulus, their deposition can also increase the microhardness of the coating, as was shown previously in the case of ZnSe and ZnS [47].

In the current work, we increased the ITO surface area due to the deposition of carbon nanotubes. A correlation of the control field during the deposition process with the relief parameters was obtained. The relief parameters were related to the value of the wetting angle.

2. Materials, methods and theoretical background

The K8 crown glasses were used as substrates. ITO films were sequentially deposited on them by laser-oriented method, and then single-walled carbon nanotubes (CNTs) were deposited in a varied average electric field from 0 to 600 $V \cdot cm^{-1}$. Powder $(In_2O_3)_{0.9}$–$(SnO_2)_{0.1}$ with a purity of 99.99 % was used. CNTs had a diameter of 0.7–1.1 nm (No. 704121, Aldrich catalog). The deposition technique and ITO diagnostics is presented in more detail in the paper [48]. For deposition of carbon nanotubes, a CO_2laser was used in a quasi-continuous mode ($\lambda = 10{,}6$ μm, $W = 30$ W, spot diameter was 5 mm).

The relief was measured by contact method of atomic force microscopy (Solver Next NT-MDT). Scanning area was 30 × 30 μm, scanning frequency was 1 Hz. The results were processed in the Nova Px program. Roughness parameters were recalculated in

accordance with the standard [49] in the Image Analysis P9 image processing module [50]. The height of the AFM profile was measured on a two-dimensional grid of 256×256 points. The resulting sample was ranked in height, and statistical parameters were calculated. The normal distribution, which describes the distribution of the deposited film thickness in vacuum methods with sufficient accuracy, was taken as a basis.

To numerically characterize the homogeneity of the coating relief, the average roughness S_a was used:

$$S_a = \frac{1}{mn}\sum_{i=1}^{m}\sum_{j=1}^{n}|f(x,y)|. \quad (1)$$

Here, $m = n = 256$ is the number of split points along x and y axes, respectively, $z = f(x, y)$ is the profile height sample measured with an atomic force microscope.

The normal distribution is characterized by the mathematical expectation $\bar{f}$ and dispersion σ^2. In the case of atomic force microscopy, the absolute value of the mathematical expectation is not informative enough, since an arbitrary point within the profile can be taken as the reference point in height. The dispersion is associated with the root-mean-square roughness S_q, which is recalculated from the profile height sample as follows:

$$S_q = \sqrt{\mu_2} = \sigma = \sqrt{\frac{1}{mn}\sum_{i=1}^{m}\sum_{j=1}^{n}\left(f(x,y)-\bar{f}\right)^2}. \quad (2)$$

Since deviations from the ideal case are observed in a real experiment, it is advisable to use higher-order statistical parameters: skewness S_{sk} and kurtosis S_{ku}:

$$S_{sk} = \frac{\mu_3}{(\mu_2)^{3/2}} = \frac{\mu_3}{\sigma^3} = \frac{\frac{1}{mn}\sum_{i=1}^{m}\sum_{j=1}^{n}\left(f(x,y)-\bar{f}\right)^3}{\left(\frac{1}{mn}\sum_{i=1}^{m}\sum_{j=1}^{n}\left(f(x,y)-\bar{f}\right)^2\right)^{3/2}}; \quad (3)$$

$$S_{ku} = \frac{\mu_4}{(\mu_2)^2} = \frac{\mu_4}{\sigma^4} = \frac{\frac{1}{mn}\sum_{i=1}^{m}\sum_{j=1}^{n}\left(f(x,y)-\bar{f}\right)^4}{\left(\frac{1}{mn}\sum_{i=1}^{m}\sum_{j=1}^{n}\left(f(x,y)-\bar{f}\right)^2\right)^2}. \quad (4)$$

When ranking the sample $z = f(x, y)$ according to the frequency of repetitions, the left tail of the distribution corresponds to depressions, and the right tail corresponds to ridges. With a negative skewness, the relief roughness is characterized by a large number of low ridges and a small number of deep depressions, and vice versa with positive values. At $S_{sk} = 0$, a symmetric case is observed. The kurtosis characterizes the sharpness of the peak in the distribution density. At a normal distribution $S_{ku} = 3$. At $S_{ku} > 3$ and above, the sharpness of the peak increases, and at $S_{ku} < 3$ and below, the peak becomes flatter.

The relief diagnostics on a macro scale was carried out by measuring the wetting angle using hanging drop method. Drops of distilled water with a volume of 1 μl were deposited on the surface of samples with structured ITO coatings for 1 second. The whole process was recorded by a CCD camera at a frequency of 60 fps. Using the SCA20 software, the contact boundary was determined, the droplet boundary was approximated, and the contact wetting angle was recalculated. The OSA 15 EC device for carrying out the above procedure is shown in Fig. 1.

It should be noted that the method of measuring the wetting angle θ by sessile drop method is classically used for express surface diagnostics. When a drop spreads, the contact area of the liquid with the solid body and with the surrounding environment increases, and surface tension forces also work, which is illustrated in Fig. 2.

The change in free energy dF is equal to the work done by surface tension forces dW, and can also be expressed in terms of the change in the spreading area [51]:

$$dF = dW = \sigma dS, \quad (5)$$

where σ is the surface tension coefficient at the interface of three phases, which is numerically equal to the superposition of surface tension forces in the projection onto the spreading plane reduced to unit length:

$$\sigma = \frac{\left(d\overrightarrow{F_{sl}} + d\overrightarrow{F_{lg}} + d\overrightarrow{F_{sg}}\right)\overrightarrow{e_R}}{dr} = \sigma_{sl} + \sigma_{lg}\cos\theta - \sigma_{sg}. \quad (6)$$

Here, σ_{sl}, σ_{lg} and σ_{sg} are surface tension coefficients at the solid-liquid, liquid-gas, and solid-gas interfaces, respectively, and θ is the wetting angle.

According to Fig. 1 (II), the change in area depends on the wetting angle and drop size:

$$dS = 2\pi R\sin\theta dR. \quad (7)$$

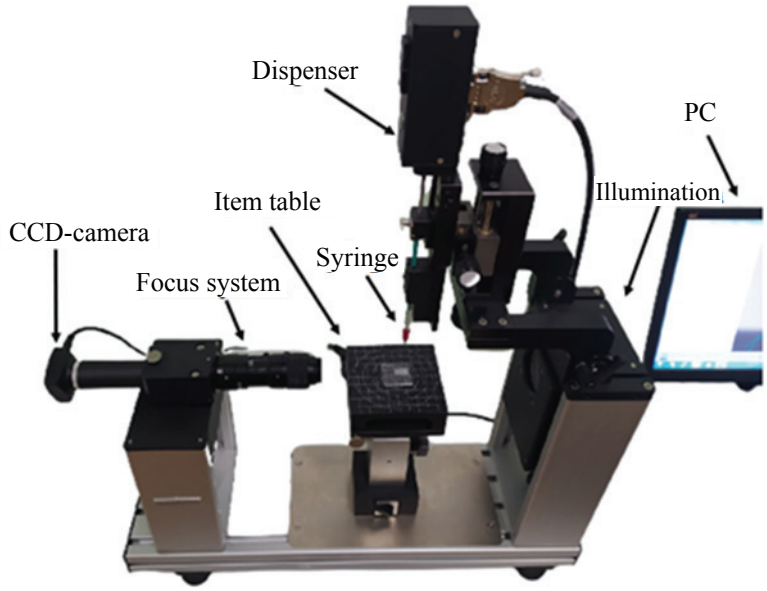

Fig. 1. System for optical registration of the wetting angle OSA 15 EC (DataPhysics)

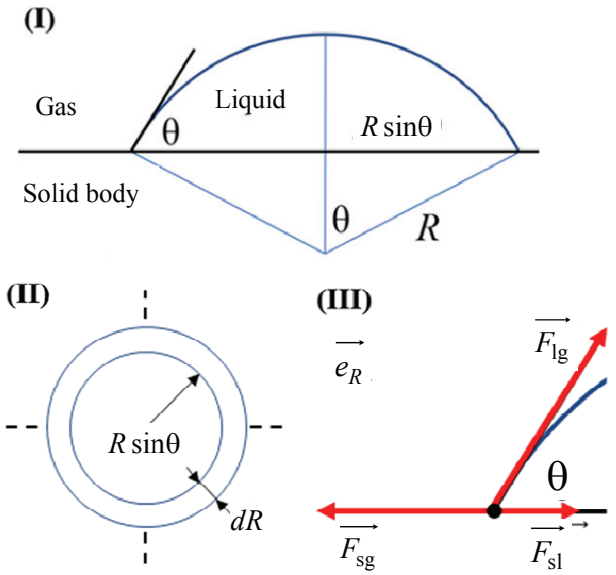

Fig. 2. Sessile drop method: (I) wetting angle θ, (II) change in the drop area during spreading, (III) direction of surface tension coefficients at the interface of three phases

In the equilibrium state, the free energy takes on a minimum value and does not change, therefore $dF = dW = 0$. In this case, by substituting (6) into (5), it is possible to express the wetting angle in terms of surface tensions and obtain the Young formula [52]:

$$\cos\theta = \frac{\sigma_{sl} - \sigma_{sg}}{\sigma_{lg}}. \qquad (8)$$

This approach succinctly describes the case of a smooth homogeneous surface of a solid body.

In this paper, we propose to supplement the described approach for the case with a *rough* surface and consider the surface of ITO films with deposited carbon nanotubes in more detail.

In the real case, the surface of a solid body is rough, which means that the surface area is higher than in the ideal case. Graphically, this is shown in Fig. 3.

Analytically, the surface area is determined through the functional dependence of the height $z = f(x, y)$ [53]:

$$dS_{real} = \sqrt{1 + \left(\frac{\partial f(x,y)}{\partial x}\right)^2 + \left(\frac{\partial f(x,y)}{\partial y}\right)^2}\, dxdy\,. \qquad (9)$$

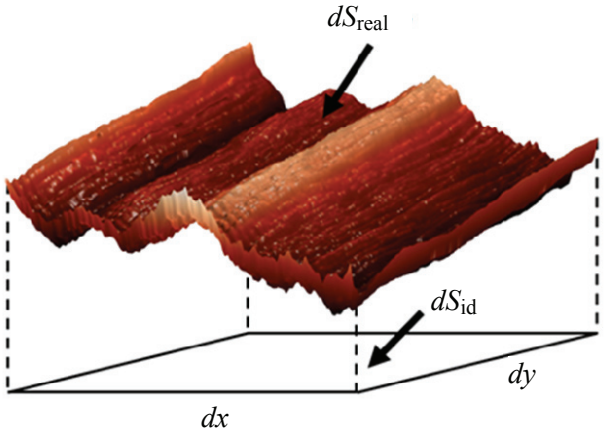

Fig. 3. Demonstrated difference between the surface area of a real ITO film and a perfectly smooth surface

Since, in practice, the surface profile is measured by points, using a second-order difference relation, it is possible to do the point partition. Let us denote the ratio of the real surface area to the ideal one through the surface roughness coefficient:

$$K_s = \frac{S_{real}}{S_{id}} = \sum_{i=1}^{m}\sum_{j=1}^{n}\sqrt{1+\left|L_x[f(x,y)]\right|+\left|L_y[f(x,y)]\right|}, \quad (10)$$

where $L_x[f(x,y)]$ and $L_y[f(x,y)]$ are second-order difference relations in x and y coordinates:

$$L_x[f(x,y)] = \frac{f(x_{i-1},y_i)-2f(x_i,y_i)+f(x_{i+1},y_i)}{(\Delta x)^2}; \quad (11a)$$

$$L_y[f(x,y)] = \frac{f(x_i,y_{i-1})-2f(x_i,y_i)+f(x_i,y_{i+1})}{(\Delta y)^2}. \quad (11b)$$

It should be noted that the described roughness is a property of a solid body, therefore, in the expression for changing the free energy, this parameter will be used for σ_{sg} and σ_{sl}:

$$dF = (\sigma_{sl}-\sigma_{sg})K_s ds + \sigma_{lg}\cos\theta ds. \quad (12)$$

Thus, from the equilibrium condition, the following expression for the wetting angle can be obtained taking into account the surface roughness:

$$\cos\theta' = K_s\frac{\sigma_{sl}-\sigma_{sg}}{\sigma_{lg}} = K_s\cos\theta. \quad (13)$$

According to expression (10), $K_s = 1$ in the case of an ideal smooth surface, and $K_s > 1$ in the case of a rough one.

3. Results and discussion

In laser-oriented deposition method, the material from the source substrate is sputtered under the action of a temperature gradient in a solid angle of 2π. Since the source substrate is heated unevenly during laser exposure, the number of particles deposited on the quartz substrate decreases as it deviates from its center. Directional deposition can be achieved by changing the distance from the grid to the upper carousel with samples, which also determines the magnitude of the control electric field.

During the ITO deposition, films with an average roughness of 2 nm or less are formed. The difference between the maximum height and maximum depth within the scanned sample is on the order of 10 nm. Carbon nanotubes under current conditions are deposited in the form of clusters with a height of about 60 nm. Depending on the magnitude of the electric field strength on the control contact grids, it is possible to influence the relief shape of the modified ITO surface (Fig. 4).

In this case, it is possible to rearrange the height distribution along the surface of samples. With an increase in the control field, an increase in roughness is observed (Table 1).

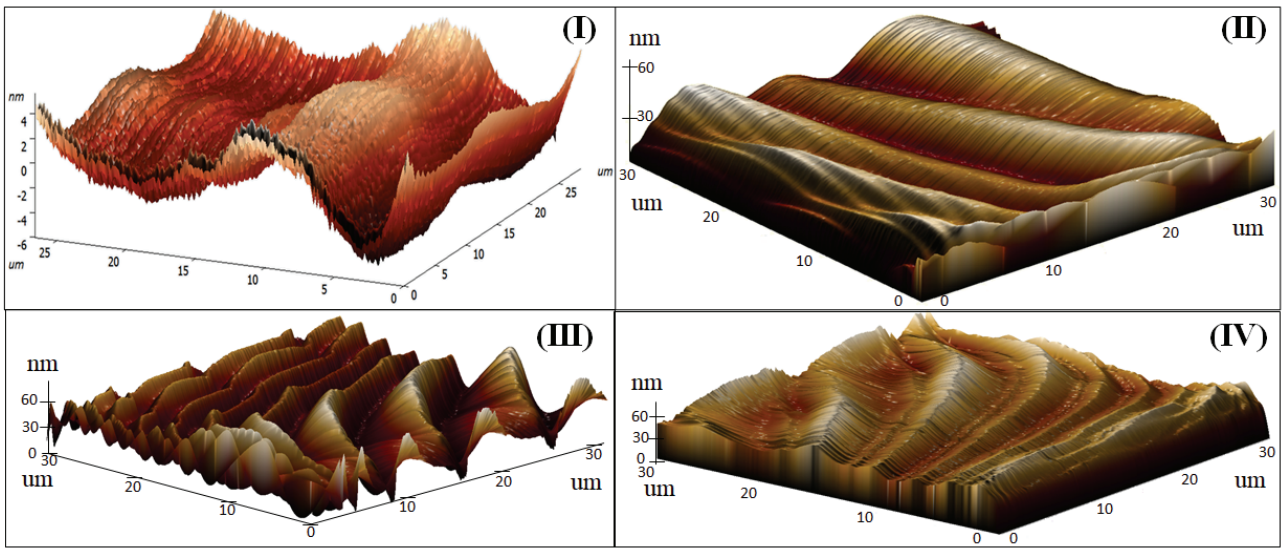

Fig. 4. Atomic force profiles of pure ITO surface (I) and ITO surface with deposited carbon nanotubes at different average electric field strengths: 100 V·cm^{-1} (II), 200 V·cm^{-1} (III), and 600 V·cm^{-1} (IV)

Table 1. Relief parameters of ITO films with deposited carbon nanotubes at different average electric field strengths

Parameter	Pure ITO	ITO + CNT with different electric field E, V·cm^{-1}		
		100	200	600
Average roughness S_a, nm	1.8	6.4	15.6	22.1
RMS roughness S_q, nm	2.2	7.9	12.2	27.4
Skewness S_{sk}	0.02	–0.03	0.04	0.24
Kurtosis S_{ku}	2.4	2.5	3.4	3.2

It should be noted that with increasing control field strength, the roughness S_a and S_q increase. At $E = 200$ V·cm^{-1} and $E = 600$ V·cm^{-1}, the kurtosis is higher than 3, which means that the distribution peak in the vicinity of the mathematical expectation is sharper than in the case of a normal distribution, which can be associated with a more ordered deposition of carbon nanotubes on the ITO surface. The skewness at $E = 600$ V·cm^{-1} characterizes roughness associated with the influence of the number and magnitude of depressions in the relief.

The measured AFM profiles were imported into the MATLAB R2021a software and, in accordance with expressions (10)–(11), the surface roughness coefficient was calculated, and a prediction was made for the wetting angle using formula (13). A clean ITO coating with $\theta = 102.8°$ was taken as a smooth surface (Table 2).

When measuring the wetting angle, the same trend was found (Fig. 5); its value increases with increasing surface in homogeneity, which can be controlled by the electric field during the deposition of carbon nanotubes (Table 3).

When the surface is structured with carbon nanotubes, in addition to the relief, the composition also changes; therefore, the surface tension coefficients differ.

Table 2. Calculation of the surface roughness coefficient and wetting angle

Parameter	Pure ITO	ITO + CNT with different electric field E, V·cm^{-1}		
		100	200	600
Roughness coefficient, K_s	1.012	1.595	2.533	3.004
Predicted wetting angle θ', deg	102.8 (measured)	110.7	124.1	131.7

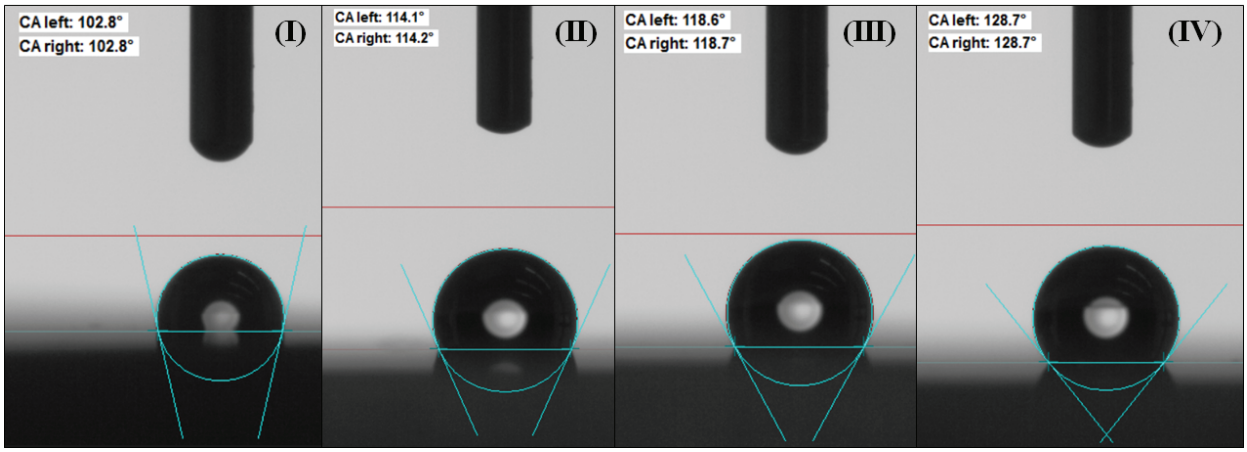

Fig. 5. Wetting angle of pure ITO surface (I) and ITO surface with deposited carbon nanotubes at different average electric field strengths: 100 V·cm^{-1} (II), 200 V·cm^{-1} (III), and 600 V·cm^{-1} (IV)

Table 3. Statistics of the wetting angle on the ITO film surface with deposited CNTs at different electric field strengths

Wetting angle parameter, °	Pure ITO	ITO + CNT with different electric field E, V·cm^{-1}		
		100	200	600
Mean value	101.8	115.0	119.8	128.6
Minimum value	99.3	111.5	115.6	128.0
Maximum value	102.9	117.6	125.4	129.0

4. Conclusion

Thus, based on the experimental data on atomic force microscopy and measurement of the wetting angle, taking into account the experiments and calculations performed, the following conclusions can be formulated:

1. Laser-oriented deposited carbon nanotubes are a scaffold that increases the surface roughness of the matrix material, in this case, ITO.

2. During deposition of carbon nanotubes, it is possible to control the relief parameters using an electric field on contact grids. As the tension increases, the roughness parameters S_a, S_q and K_s increase. At the same time, there is a tendency to an increase in the wetting angle with an increase in surface inhomogeneity. Thus, a clear correlation has been established between the surface roughness and the wetting angle.

3. The results obtained indicate a decrease in the adhesion energy to the surface of the structured ITO film, making it more resistant to moisture, which is important when working with optical equipment.

4. The results obtained and discussed can significantly expand the scope of ITO conductive contacts, not only for the field of general optoelectronics, but also for laser, biomedical and display technology.

5. Funding

This study is an initiative, however, it was partly funded by the Innovation Promotion Foundation, grant No. [*72598/C1-112174*].

6. Acknowledgments

The authors are grateful to their colleagues at Vavilov State Optical Institute and Petersburg Nuclear Physics Institute for the fruitful discussion of the results.

7. Conflict of interest

The authors declare no conflict of interest.

References

1. Liu Q, Sun J, Sun Y, Ren Z, Liu C, Lv J, Wang F, Wang L, Liu W, Sun T, Chu P. Surface plasmon resonance sensor based on photonic crystal fiber with indium tin oxide film. *Optical Materials*. 2020;102:109800(1-8). DOI:10.1016/j.optmat.2020.109800

2. Tian W, Liang Fei, Lu D, Yu H, Zhang H. Highly efficient ultraviolet high-harmonic generation from epsilon-near-zero indium tin oxide films. *Photonics Research*. 2021;9(3):317-323. DOI:10.1364/PRJ.414570

3. Haschke J, Lemerle R, Aissa B, Abdallah AA, Kivambe MM, Boccard M, Ballif C. Annealing of silicon heterojunction solar cells: interplay of solar cell and indium tin oxide properties. *IEEE Journal of Photovoltaics*. 2019; 9(5):1202-1207. DOI:10.1109/jphotov.2019.2924389

4. Song Q, Lin T, Sun X, Chu B, Su Z, Yang H, Lee CS. Electronic level alignment at an indium tin oxide/PbI_2 interface and its applications for organic electronic devices. *ACS Applied Materials & Interfaces*. 2018;10(10): 8909-8916. DOI:10.1021/acsami.7b19376

5. Yan T, Hong R, Tao C, Wang Qi, Lin H, Han Z, Zhang D. Thickness dependency of PVA on the transition from saturable absorption to reverse saturable absorption of ITO films. *Optical Materials*. 2022;125(10):112061(1-7). DOI:10.1016/j.optmat.2022.112061

6. Hu R, Su X, Liu H, Liu Y, Huo M M, Zhang W.Recycled indium tin oxide transparent conductive electrode for polymer solar cells. *Journal of Materials Science*. 2020;55(25):11403-11410. DOI: 10.1007/s10853-020-04825-x

7. Bett AJ, Winkler KM, Bivour M, Cojocaru L, Kabakli ÖŞ, Schulze PSC, Siefer G, Tutsch L, Hermle M, Glunz SW, Goldschmidt JC. Semi-transparent perovskite solar cells with ITO directly sputtered on spiro-OMeTAD for tandem applications. *ACS Applied Materials and Interfaces*. 2019;11(49):45796-45804. DOI:10.1021/acsami.9b17241

8. Bellam JB, Kandikunta G, Manupati B, Debabrata S, George PP, Vedanayakam SV, Verma VK. DC sputter

deposited TiO_2 thin film on ITO/glass substrate for perovskite based solar cell application. *Materials Today: Proceedings*. 2019;45(4):3886-3890. DOI:10.1016/j.matpr.2020.06.281

9. Du G, Bai Y, Huang J, Zhang J, Wang J, Lin Y, Lu L, Yang L, Bao S, Huang Z, Chen X, Yin M, Li D. Surface passivation of ITO on heterojunction solar cells with enhanced cell performance and module reliability. *ECS Journal of Solid State Science and Technology*. 2021;10:035008(1-8). DOI: 10.1149/2162-8777/abeece

10. Lee SJ, Lee SH, Kang HW, Nahm S, Kim BH, Kim H, Han SH. Flexible electrochromic and thermochromic hybrid smart window based on a highly durable ITO/graphene transparent electrode. *Chemical Engineering Journal*. 2021;416:129028(1-8). DOI:10.1016/j.cej.2021.129028

11. Bao SY, Deng X, Mao F, Zhong Ni, Yue FY, Sun L, Xiang PH, Duan CG. Ultra-flat ITO films on mica for high temperature transparent flexible electrodes. *Ceramics International*. 2020;46(2):2268-2272. DOI: 10.1016/j.ceramint.2019.09.215

12. Raman V, Cho Y-H, Park J-H, Chinnadurai D, Kim H-K. Impact of low temperature plasma annealing for flexible, transparent and conductive ITO/PEDOT:PSS composite electrode. *Journal of Industrial and Engineering Chemistry*. 2021;93(25):423-429. DOI:10.1016/j.jiec.2020.10.021

13. Bok S, Seok H-J, Kim YA, Park J-H, Kim J, Kang J, Kim H-K, Lim B. Transparent molecular adhesive enabling mechanically stable ITO thin films. *ACS Applied Materials and Interfaces*. 2021;13(2):3463-3470. DOI: 10.1021/acsami.0c20582

14. Shin SR, Lee HB, Jin WY, Ko KJ, Park, Yoo S, Kang JW. Improving light extraction of flexible OLEDs using a mechanically robust Ag mesh/ITO composite electrode and microlens array. *Journal of Materials Chemistry C*. 2018;6(20):5444-5452. DOI:10.1039/C8TC01415A

15. Zheng J, Chow HC, Li S, Wang J, Saho L. Electrophoretic plasmonic ink for dynamic color display. *Advanced Optical Materials*. 2021;9(12):2100091(1-10). DOI:10.1002/adom.202100091

16. Chu F, Wang D, Liu C, Li L, Wang Q-H. Multi-view 2D/3D switchable display with cylindrical liquid crystal lens array. *Crystals*. 2021;11:715(1-10). DOI: 10.3390/cryst11060715

17. Wang W, Guan Z, Xu H. A high speed electrically switching reflective structural color display with large color gamut. *Nanoscale*. 2021;13(2):1164-1171. DOI:10.1039/d0nr07347d

18. Way A, Luke J, Evans AD, Li Z, Kim JS, Durrant JR, Lee HK, Tsoi WC. Fluorine doped tin oxide as an alternative of indium tin oxide for bottom electrode of semi-transparent organic photovoltaic devices. *AIP Advances*. 2019;9:085220(1-5). DOI:10.1063/1.5104333

19. Huang S, Dong Q, Lu Y, Duan L, Zhang D. Outstanding performance of electron-transport-layer-free perovskite solar cells using a novel small-molecule interlayer modified FTO substrate. *Chemical Engineering Journal*. 2021;422:130001(1-12). DOI:10.1016/j.cej.2021.130001

20. Niemelä J-P, Macco B, Barraud L, Descoeudres A, Badel N, Despeisse M, Christmann G, Nicolay S, Ballif C, Kessels WMM, Creatore M. Rear-emitter silicon heterojunction solar cells with atomic layer deposited ZnO:Al serving as an alternative transparent conducting oxide to In_2O_3:Sn. *Solar Energy Materials and Solar Cells*. 2019;200:109953(1-5). DOI:10.1016/j.solmat.2019.109953

21. Saini S, Mele P, Oyake T, Shiomi J, Niemelä J-P, Karppinen M, Miyazaki K, Li C, Kawaharamura T, Ichinose A, Molina-Luna L. Porosity-tuned thermal conductivity in thermoelectric Al-doped ZnO thin films grown by mist-chemical vapor deposition. *Thin Solid Films*. 2019;685(1):180-185. DOI:10.1016/j.tsf.2019.06.010

22. Macco B, van de Loo BWH, Dielen M, Loeffen DGJA, van Pelt BB, Phung N, Melskens J, Verheijen MA, Kessels WMM. Atomic-layer-deposited Al-doped zinc oxide as a passivating conductive contacting layer for n^+-doped surfaces in silicon solar cells. *Solar Energy Materials and Solar Cells*. 2021;233:111386(1-13). DOI:10.1016/j.solmat.2021.111386

23. Bi Y-G, Liu Y-F, Zhang X-L, Yin D, Wang W-Q, Feng J, Sun H-B. Ultrathin metal films as the transparent electrode in ITO-free organic optoelectronic devices. *Advanced Optical Materials*. 2019;7:1800778(1-23). DOI: 10.1002/adom.201800778

24. Seo K-W, Lee J, Jo J, Cho C, Lee J-Y. Highly efficient (>10 %) flexible organic solar cells on PEDOT-free and ITO-free transparent electrodes. *Advanced Materials*. 2019;31(36):1-20. DOI:10.1002/adma.201902447

25. Huang J, Ren Z, Zhang Y, Liu K, Zhang H, Tang H, Yan C, Zhen Z, Li G. Stretchable ITO-free organic solar cells with intrinsic anti-reflection substrate for high-efficiency outdoor and indoor energy harvesting. *Advanced Functional Materials*. 2021;31:2010172(1-11). DOI:10.1002/adfm.202010172

26. Agnihotri SK, Prashant DV, Samajdar DP, Arefinia Z. Performance analysis of ITO-free PEDOT:PSS/InP nanowire hybrid solar cell. *Solar Energy*. 2021;228:418-426. DOI:10.1016/j.solener.2021.09.078

27. Tegegne NA, Wendimu H, Abdissa Z, Mammo W, Andersson MR, Hone FG, Andoshee DM, Olaoye O, Bosman G. Light-induced degradation of a push-pull copolymer for ITO-free organic solar cell application. *Journal of Material Science: Materials in Electronics*. 2020;31:21303-21315. DOI:10.1007/s10854-020-04642-7

28. Bacon-Brown DA, Braun PV. Tunable antireflection coating to remove index-matching requirement for interference lithography. *Advanced Optical Materials*. 2018;6:1701049(1-13). DOI:10.1002/adom.201701049

29. Toikka AS, Lomova LS, Kamanina NV. Effect of WS_2 nanoparticles on the refractive properties of liquid crystal compositions. *Journal of Optical Technology*. 2021;88(8):460-463. DOI:10.1364/JOT.88.000460

30. Xu Q, Zhao Y, Zhang X. Light management in monolithic perovskite/silicon tandem solar cells. *Solar RRL*. 2020;4:1900206(1-16). DOI:10.1002/solr.201900206

31. Chapa M, Alexandre M F, Mendes M J, Aguas H, Fortunato E, Martins R. All-thin-film perovskite/C-Si four-terminal tandems: interlayer and intermediate contacts optimization. *ACS Applied Energy Materials*. 2019;2(6):3979-3985. DOI:10.1021/acsaem.9b00354

32. Hsu CJ, Agrahari K, Selvaraj P, Chiang WF, Huang CY, Manohar R, Huang CY. Application of ultra-thin indium–tin–oxide film in liquid crystal lens. *Optics and Laser Technology*. 2019;119:105603(1-7). DOI: 10.1016/j.optlastec.2019.105603

33. Chu F, Tian LL, Li R, Gu X-Q, Zhou X-Y, Wang D, Wang Q-H. Adaptive nematic liquid crystal lens array with resistive layer. *Liquid Crystals*. 2020;47(4):563-571. DOI:10.1080/02678292.2019.1662502

34. Sahu BB, Wen L, Kim LW, Han JG. Study of plasma characteristic and properties of flexible ultra-thin ITO films prepared by large area 3D confined and planar magnetron sputtering. *Vacuum*. 2019;165:246-253. DOI: 10.1016/j.vacuum.2019.04.029

35. Kudryashov DA, Maksimova AA, Vyacheslavova EA, Uvarov AV, Morozov IA, Baranov AI, Monastyrenko AO, Gudovskih AS. Investigation of design parameters of a magnetron sputtering setup on the electrical and optical properties of indium-tin oxide films. *Fizika i tekhnika poluprovodnikov = Semiconductors*. 2021; 55(4):360-364. DOI:10.21883/FTP.2021.04.50741.9561 (In Russ.)

36. Ferhati H, Djeffal F, Benhaya A. Optimized high-performance ITO/Ag/ITO multilayer transparent electrode deposited by RF magnetron sputtering. *Superlattices and Microstructures*. 2019;129:176-184. DOI:10.1016/j.spmi. 2019.03.027

37. Sofi AH, Shah MA, Asokan K. Structural, optical and electrical properties of ito thin films. *Journal of Electronic Materials*. 2018;47(2):1344-1352. DOI:10.1007/ s11664-017-5915-9

38. Demirhan Y, Koseoglu H, Turkoglu F, Uyanik Z, Ozdemir M, Aygun G, Ozyuzer L. The controllable deposition of large area roll-to-roll sputtered ITO thin films for photovoltaic applications. *Renewable Energy*. 2020;146:1549-1559. DOI:10.1016/j.renene.2019.07.038

39. Dong L, Zhu GS, Xu HR, Jiang XP, Zhang XY, Zhao YY, Yan DL, Yuan L, Yu AB. Preparation of indium tin oxide (ITO) thin film with (400) preferred orientation by sol-gel spin coating method. *Journal of Materials Science: Materials in Electronics*. 2019;30:8047-8054. DOI:10.1007/s10854-019-01126-1

40. Ahmed M, Bakry A, Qasem A, Dalir H. The main role of thermal annealing in controlling the structural and optical properties of ITO thin film layer. *Optical Materials*. 2021;113:110866(1-32). DOI:10.1016/ j.optmat.2021.110866

41. Seong S, Jung YC, Lee T, Park I-S, Ahn J. Enhanced uniformity in electrical and optical properties of ITO thin films using a wide thermal annealing system. *Materials Science in Semiconductor Processing*. 2018;79(1):14-19. DOI:10.1016/j.mssp.2018.01.015

42. Kamanina NV, Likhomanova SV, Kuzhakov PV. Advantages of the surface structuration of KBr materials for spectrometry and sensors. *Sensors*. 2018;18(9):1-8. DOI:10.3390/s18093013

43. Kamanina N, Kuzhakov P, Kukharchik A, Kvashnin D. A nanostructuring approach for modification of the features of optical materials: lithium fluoride. *IOP Conference Series: Materials Science and Engineering*. 2019;693:012008(1-7). DOI:10.1088/1757-899X/693/ 1/012008

44. Kamanina N, Kuzhakov P, Kvashnin D. Novel perspective coatings for the optoelectronic elements: features of the carbon nanotubes to modify the surface relief of BaF_2 materials. *Coatings*. 2020;10(7):1007066(1-10). DOI:10.3390/coatings1007066

45. Kamanina NV, Vasilyev PY, Studeonov VI. *Optical coating based on oriented in the electric field CNTs for the optical devises, micro- and nanoelectronics under the conditions when the interface: solid substrate-coating can be eliminated.* Russian Federation patent 2,405,177. 27 November 2010. (In Russ.).

46. Kamanina N, Toikka A, Gladysheva I. ITO conducting coatings properties improvement via nanotechnology approach. *Nano Express*. 2021;2:010006(1-7). DOI:10.1088/2632-959X/abd90c

47. Kamanina N, Toikka A, Valeev B, Kvashnin D. Carbon Nanotubes use for the semiconductors ZnSe and ZnS material surface modification via the laser-oriented deposition technique. *C – Journal of Carbon Research*. 2021;7(4):1-10. DOI:10.3390/c7040084

48. Toikka AS, Kamanina NV. Laser-vacuum deposited ITO thin films for optoelectronic applications. *Technium Romanian Journal of Applied Sciences and Technology*. 2021;3(7):154-160. DOI:10.47577/technium. v3i7.4594

49. National standard of the Russian Federation. GOST R ISO 25178-2-2014. *Geometric characteristics of products (GPS). Surface structure. Part 2. Terms, definitions and parameters of the surface structure*. Moscow: Standartinform; 2014. (In Russ.)

50. Reference guide. *Image processing module image analysis P9*. Zelenograd: NT-MDT; 2011. (In Russ.)

51. Mityuhin SI, FrolenkovKYu. Measurement of the wetting angle as a method for studying the adhesion properties of the surface of the molecule energy state at the interface between two phases. *Kondensirovannye sredy i mezhfaznye granicy.* 2003;5(2):216-220 (In Russ.)

52. Hebbar RS, Isloor AM, Ismail AF. In: Hilal N, Ismail AF, Matsuura T, Oatley-Radcliffe D (eds.) *Membrane Characterization*. Amsterdam: Elsevier; 2017, p. 219-255.

53. Taktarov NG. *Handbook of higher mathematics for university students*. Moscow: LIBROKOM; 2019. 880 p. (In Russ.)

Информация об авторах / Information about the authors

Андрей Сергеевич Тойкка, лаборант, Государственный оптический институт им. С. И. Вавилова; студент магистратуры, Санкт-Петербургский государственный электротехнический университет «ЛЭТИ» им. В. И. Ульянова (Ленина), Санкт-Петербург, Российская Федерация; младший научный сотрудник, Петербургский институт ядерной физики им. Б. П. Константинова Национального исследовательского центра «Курчатовский институт», Гатчина, Российская Федерация; ORCID 0000-0002-8694-8497, e-mail: atoikka@obraz.pro

Andrei S. Toikka, Laboratory Assistant, Vavilov State Optical Institute; Master Student, Saint Petersburg Electrotechnical University, St. Petersburg, Russian Federation; Junior Researcher, Petersburg Nuclear Physics Institute named by B.P. Konstantinov of National Research Centre "Kurchatov Institute", Gatchina, Russian Federation; ORCID 0000-0002-8694-8497, e-mail: atoikka@obraz.pro

Наталия Владимировна Каманина, доктор физико-математических наук, заведующий отдела, Государственный оптический институт им. С. И. Вавилова; профессор, Санкт-Петербургский государственный электротехнический университет «ЛЭТИ» им. В. И. Ульянова (Ленина), Санкт-Петербург, Российская Федерация; ведущий научный сотрудник, Петербургский институт ядерной физики им. Б. П. Константинова Национального исследовательского центра «Курчатовский институт», Гатчина, Российская Федерация; ORCID 0000-0002-2903-2685, e-mail: nvkamanina@mail.ru

Natalia V. Kamanina, D. Sc. (Physics and Mathematics), Head of Department, Vavilov State Optical Institute; Professor, Saint Petersburg Electrotechnical University, St. Petersburg, Russian Federation; Principal Researcher, Petersburg Nuclear Physics Institute named by B.P. Konstantinov of National Research Centre "Kurchatov Institute", Gatchina, Russian Federation; ORCID 0000-0002-2903-2685, e-mail: nvkamanina@mail.ru

Received 14 January 2022; Accepted 01 March 2022; Published 14 April 2022